Proceedings World Geothermal Congress 2023
Beijing, China, April 17 – 21, 2023

Evaluation of Geothermal Resource Potential Based on Geographic Information System (GIS) Integration Models: Case Study of Xiong'an New Area, North China

Tingting Ke[a,b], Shaopeng Huang[c], Wei Xu[d], Yang Zhou[a,b], Jianqiang Liu[a,b], Qinyu Meng [a,b]

[a] Shaanxi Hydrogeology Engineering Geology and Environment Geology Survey Center, Xi'an, 710068, China

[b] Shaanxi Engineering Technology Research Center for Urban Geology and Underground Space, Xi'an, 710068, China

[c] Institute of Deep Earth Science and Green Energy, Shenzhen University, Shenzhen, 518960, China

[d] School of Human Settlements and Civil Engineering, Xi'an Jiaotong University, Xi'an, 710049, China

Email: ke_ting_ting@163.com

Keywords: Geothermal Favorability map, Spatial Data Integration Model, Multi-criteria Decision Analysis, Geothermal Potential

ABSTRACT

To alleviate the energy depletion and environmental pollution, it is urgent to promote the development of renewable energy. As one of the most realistic and competitive renewable energy, geothermal resources have the advantages of abundant reserves, wide distribution, stable supply, and high utilization efficiency. The development of geothermal resources is increasingly valued by governments and industries. Recognizing the favorable geothermal areas is conducive to reduce the economic risk of geothermal exploitation projects. This work is based on a case study from Xiong'an New Area, North China, which is rich in geothermal fluids in carbonate reservoirs. Three spatial data integration models (the Weights of Evidence Model, the Weighted Information Content Model and the Index Overlay Model) are established in Geographic Information System (GIS) environment to evaluate the geothermal resource potential of Xiong'an New Area. Faults distribution, Bouguer gravity anomaly, magnetic anomaly, geothermal gradient and terrestrial heat flow are five geothermal evidence factors. Based on the five criteria layers generated from the evidence factors, the geothermal favorability map is developed by analyzing the spatial association between the known geothermal occurrences and the evidence factors. The performance of the model is evaluated by kappa coefficient analysis, success index analysis and receiver operating characteristic curve analysis. The results reveal that the Weighted Information Content Model is more effective and accurate. The geothermal favorability map is classified into four classes. The extremely high favorable area and the high favorable area in Xiong'an New Area cover 105.78 km^2 and 145.27 km^2, accounting for 6% and 8% of the total area, respectively. Moreover, the amount of thermal energy in four classes of geothermal favorable areas is also calculated by the unit volumetric method. The insights from this study provide a low-cost and efficient approach for evaluating the geothermal potential of regions lacking sufficient exploration data.

1. INTRODUCTION

Traditional fossil energy dominated by coal, oil and natural gas accounts for more than 80% of the global energy structure (British Petroleum, 2022). The utilization of traditional fossil energy has brought great pressure to national energy security and environmental governance. In 2021, the carbon dioxide emissions from energy use rise to 33,884 million tonnes, 90% of which come from traditional fossil energy use. The development of renewable energy is an urgent measure to reduce national dependence on traditional fossil energy. It can effectively mitigate the crisis of energy depletion, climate change and environmental pollution. Geothermal resources are promising renewable energy, which occur widely in rock and soil mass, fluids and magma bodies in the interior of the earth (Muffler P. and Cataldi R., 1977). The heat of geothermal resources is mainly derived from the transformation of gravitational potential energy during the formation of the earth and the decay of radioactive elements in the crust and the mantle (Rybach L. and Muffler L., 1980). Due to the advantages of large reserves, wide distribution, stable supply and high utilization efficiency, geothermal resources are considered as one of the most feasible and competitive renewable energy.

The evaluation of geothermal resource potential is a prerequisite for the rational development and utilization of geothermal resources. Since the 1980s, due to the rapid development of computer technology, geographic information system (GIS) has been gradually applied to evaluation of geothermal resources potential (Prol-Ledesma R.M., 2000). Multi-criteria decision analysis (MCDA) based on GIS environment can effectively evaluate geothermal resource potential and minimize human errors. Its main objective is to predict the favorable geothermal areas and create a geothermal favorability map. The models used for analysis can be categorized into knowledge-driven model and data-driven model (Carter B., 1994). Based on the successful application of GIS in regional exploration studies of mineral resources, Prol-Ledesma R.M. (2000) constructed three knowledge-driven models (Boolean Logic Model, Index Overlay Model and Fuzzy Data Analysis) with GIS to study the spatial correlation between the geothermal resource potential of Los Azufres geothermal field and regional geophysical and geological evidence in Mexico. Coolbaugh M.F. and Shevenell L.A. (2004) and Coolbaugh M.F. et al. (2007) established two data-driven models (Weights of Evidence Model and Logistic Regression Statistical Model) based on GIS to ascertain spatial distribution of undiscovered geothermal resources in Nevada, USA. Tuefekci N. et al. (2010) conducted a knowledge-driven model (Index Overlay Model) and a data-driven model (Weights of Evidence Model) to evaluate the spatial relationship between the favorable geothermal areas and geological, geochemical and geophysical data in Western Anatolia, Turkey. Sadeghi B. and Khalajmasoumi M.J.R. (2015) integrated the available geothermal data (volcanic and intrusive rocks, volcanoes, hot springs and faults) through the Binary Index Overlay Model and the Fuzzy Logic Model to evaluate the geothermal resources potential in northwest Iran. Francesco T. et al. (2018) used the Analytic Hierarchy Process (AHP) model to evaluate the favorable shallow geothermal resource areas in Europe. Zhang Y. et al. (2020) evaluated the favorable geothermal areas in Fujian Province, China, based on the Weights of Evidence Model and the Fuzzy Logic Model. In the above

studies, the geological, geothermal and geophysical evidence factors usually include seismic activity, Bouguer gravity anomaly, aeromagnetic anomaly, faults, intrusive rock, terrestrial heat flow, geothermal gradient, hydrothermal alteration, hot spring, etc.

The Bohai Bay Basin, one of the basins with the longest history of geothermal development and utilization in China, is rich in geothermal resources at low to medium temperature (Wang Z. et al., 2021). Xiong'an New Area is located in the north of the Bohai Bay Basin. Its geothermal resources are mainly bearing in Mesoproterozoic carbonate reservoirs with developed fractures and have been used for heating and bathing since the 1970 (Gaofan Y. et al., 2019). Since the geothermal resources are characterized by abundant reserves, shallow buried depth of bearing reservoirs, high fluid temperature and good fluid quality, Xiong'an New Area has great potentialities of geothermal development. However, the geothermal resources potential of Xiong'an New Area has not been systematically evaluated, and the favorable geothermal areas are yet to be comprehensively identified. The exploration and evaluation of the geothermal resources potential in Xiong'an New Area can provide significant information for government and industries and reduce the geothermal exploitation risk. MCDA based on GIS and combining multi-source geothermal evidence factors can effectively evaluate the potential of geothermal resources. In this study, Bouguer gravity anomaly, basement buried depth, aeromagnetic anomaly, geothermal gradient and terrestrial heat flow in Xiong'an New Area are taken as geothermal evidence factors. The spatial correlation between the geothermal anomaly areas and the above geological and geophysical factors was quantified based on GIS, and then a data-driven model (Index Overlay Model) and two knowledge-driven models (Weights of Evidence Model and Weighted Information Content Model) are constructed to identify geothermal favorable areas in Xiong'an New Area. The independence of the five geothermal evidence factors is tested by chi-square (X^2) test. The consistency, reliability and accuracy of the results are further evaluated by kappa coefficient analysis, success index (SI) analysis and receiver operating characteristic curve (ROC) analysis. Finally, the most suitable model for identifying geothermal favorable areas in Xiong'an New Area is proposed, and the amount of thermal energy contained in geothermal favorable areas is calculated using the unit volumetric method.

2.THE CASE STUDY AREA

Xiong'an New Area is established by the Chinese government in 2017, located in the middle of Hebei Province, north China (Fig. 1a). The new area is designed to cover an area of 2000 km^2, with flat terrain and an altitude of -3~26 m. Tectonically, Xiong'an New Area is located in the central uplift belt of Jizhong Depression, Bohai Bay Basin. The main tectonic units of Xiong'an New Area are Rongcheng uplift (I), Niutuozhen uplift (II), Gaoyang low uplift (III), Lixian slope (IV), Niubei slope (V), Baxian Depression (VI), Xushui Depression (VII) and Baoding Depression (IX) (Fig. 1b) (Wang Z., 2018). Due to the multiple tectonic movements, Jizhong Depression has developed a complex fault network composed of several faults with different formation stages and types. The NE trending faults have a major impact on the formation and development of the geotectonics of the new area, while the EW, NNE and NW trending faults have a secondary impact. The faults controlling the formation and development of Jizhong Depression include the Niudong fault (F1), Niunan fault (F2), Rongcheng fault (F3), Xushui fault (F4), and Gaoyang fault (F7) (Fig. 1b). The lithology of the basement in Xiong'an New Area is mainly crystalline metamorphic rock series formed after folding and metamorphism of Archean and Lower Proterozoic strata. According to the sequence of strata deposition, the strata developed in Xiong'an New Area are Cenozoic (including Quaternary, Neogene and Paleogene), Paleozoic (including Ordovician and Cambrian), Proterozoic (including Qingbaikou system, Jixian system, Changcheng system and Lower Proterozoic) and Archean (Fig. 1c) (Guo S. et al., 2019). The Wumishan Formation of the Jixian system widely distributed in Xiong'an New Area with a thickness of more than 1000 m are rich in low to medium temperature geothermal resources (Wang Z. et al., 2021). The lithology of the Wumishan Formation is mainly dolomite, containing purplish red and grayish green mudstone and argillaceous dolomite.

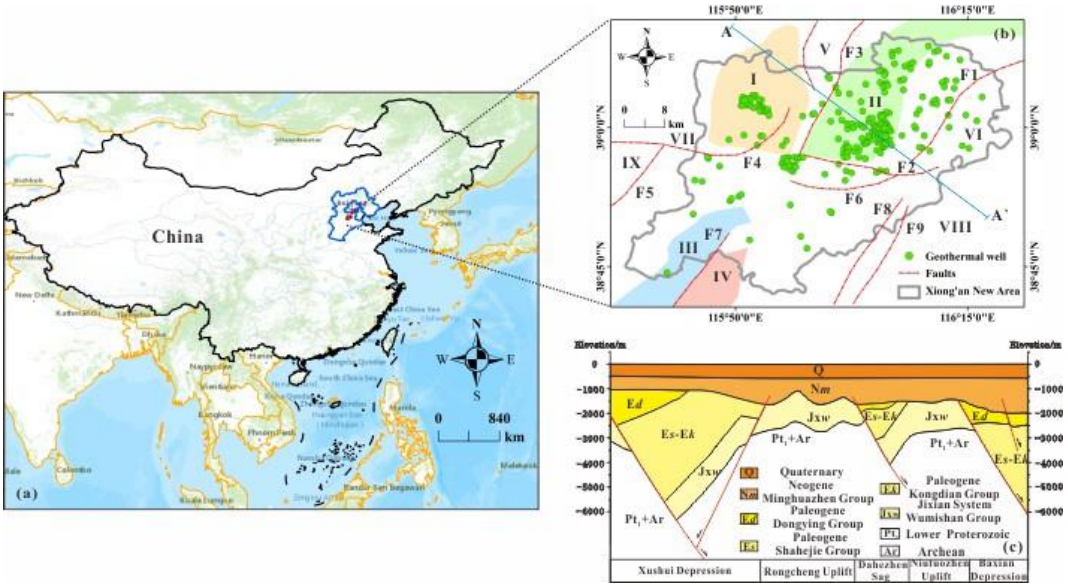

Figure 1: (a) Location of Xiong'an New Area. (b) Spatial distribution of faults and geothermal wells. (c) The geological cross-section A-A' marked in (b).

The low to medium temperature geothermal resources in Xiong'an New Area are enriched in the depth of 600~5000 m. The reservoirs are mainly Neogene sandstone reservoir and bedrock carbonate reservoir. Sandstone reservoirs are distributed in the Neogene Minghuazhen Formation and Guantao Formation. The geothermal fluid of the Minghuazhen Formation is prohibited to be exploited, and the Guantao Formation is only distributed in local areas of the new area. The Jixian system of the Wumishan Formation is widespread in Xiong'an New Area. The buried depth of the Jixian system in uplift is 600~1100 m. The carbonate reservoirs mainly

developed in the Jixian system in Xiong'an New Area. Since the permeability and thermal conductivity of the Quaternary, Neogene and Paleogene strata are lower than those of the carbonate reservoir, the heat transfer rate is greatly reduced in the above sedimentary layers. Therefore, the Quaternary, Neogene and Paleogene strata provide great cap rock conditions in Xiong'an New Area.

3.METHODOLOGY

3.1 Weights of Evidence Model

The Weights of Evidence Model (WofE) is based on Bayesian probability mathematical statistics, which was first proposed by Agterberg F.P. et al. (1990). The model can predict the favorable geothermal areas by weighting the geothermal evidence layers. The posterior probability is calculated based on the prior probability, the positive weights and negative weights. A greater posterior probability indicates a higher geothermal development potential. The positive weights and negative weights corresponding to each geothermal evidence factor are calculated by Eqs. (1) and (2) respectively:

$$W^+ = \ln \frac{P(N_P/G)}{P(N_P/\bar{G})} \tag{1}$$

$$W^- = \ln \frac{P(\bar{N}_P/G)}{P(\bar{N}_P/\bar{G})} \tag{2}$$

where W^+ is the weight coefficient of the geothermal evidence factor N_P that exists in the study area, W^- is the weight coefficient of the geothermal evidence factor N_P that does not exists in the study area, G is the number of training points

The correlation between the geothermal evidence factors and the geothermal incidents can be characterized by the contrast value $C=W^+ - W^-$. The standardized contrast $S(C)$ is calculated by Eq. (3). The ratio $C/S(C)$ can be used to determine the optimal threshold for the binary map of each geothermal evidence factor. The variances $S^2(W^+)$ and $S^2(W^-)$ in Eq. (3) are calculated by Eqs. (4) and (5), respectively. The posterior probability is calculated by Eq. (6).

$$S(C) = \frac{S^2(W^+)+S^2(W^-)}{\sqrt{S^2(W^+)+S^2(W^-)}} \tag{3}$$

$$S^2(W^+) = \frac{1}{N\{N_P \cap G\}} + \frac{1}{N\{N_P \cap \bar{G}\}} \tag{4}$$

$$S^2(W^-) = \frac{1}{N\{\bar{N}_P \cap G\}} + \frac{1}{N\{\bar{N}_P \cap \bar{G}\}} \tag{5}$$

$$P(G/N_{P1}^{\ s} \cap N_{P2}^{\ s} \cap N_{P3}^{\ s} \ldots \cap N_{Pn}^{\ s}) = \frac{O(G/N_{P1}^{\ s} \cap N_{P2}^{\ s} \cap N_{P3}^{\ s} \ldots \cap N_{Pn}^{\ s})}{1+O(G/N_{P1}^{\ s} \cap N_{P2}^{\ s} \cap N_{P3}^{\ s} \ldots \cap N_{Pn}^{\ s})} \tag{6}$$

$$\ln\left\{O(G/N_{P1}^{\ s} \cap N_{P2}^{\ s} \cap N_{P3}^{\ s} \ldots \cap N_{Pn}^{\ s})\right\} = \sum_{i=1}^{n} W_i^s + \ln O(G) \tag{7}$$

where N{·} is the number of grid cells with training points, $N_{Pn}^{\ s}$ is the number of grid cells with or without the ith evidence factor, s is + when the ith evidence factor exists, s is - when the ith evidence factor does not exist, W_i^s is weight coefficient when the ith evidence factor exists or does not exist.

The WofE model requires that all geothermal evidence factors must be independent of each other. The chi-square (χ^2) test is used to conduct conditional independence test (CI) on the evidence factors. The chi-square value is calculated by Eq. (8). The chi-square critical value can be obtained from the degree of freedom and confidence level. The chi-square value less than the chi-square critical value indicate that there is no obvious correlation between evidence factors.

$$\chi^2 = \sum \frac{(A_{RC} - T_{RC})^2}{T_{RC}} \tag{8}$$

$$T_{RC} = \frac{N_R \cdot N_C}{N} \tag{9}$$

where A_{RC} is the actual value at row R and column C, T_{RC} is the theoretical value at row R and column C, N_R is the sum of the values in row R, N_C is the sum of the values in column C, N is the sum of all values.

3.2 Weighted Information Content Model

The Weighted Information Content Model (WIC) can effectively take into account the influence of each geothermal evidence factor on geothermal occurrence. The information content value I_i of each evidence factor i and the total weighted information content value I corresponding to the evidence factor can be calculated according to Eqs. (10) and (11), respectively. The greater the total weighted information content value, the higher the possibility of geothermal resources occurring.

$$I_i = \log_2 \frac{N_{ij}/N}{S_{ij}/S} \tag{10}$$

$$I = \sum_{i=1}^{n} W_i \cdot I_i \tag{11}$$

where N_{ij} is the number of training points in the jth class of the evidence factor i, N is the total number of training points, S_{ij} is the number of grid cells in the jth class of the evidence factor i, S is the total number of grid cells.

Weight coefficient W_i is determined by information entropy theory (Shannon C.E., 1948). The matrix of geothermal density G_{ij} established by Eq. (12) is converted into probability matrix P_{ij} as shown in Eq. (13). The information entropy H_i of the evidence factor i is calculated according to Eq. (14), and the weight coefficient W_i of each evidence factor is calculated by Eq. (15).

$$G_{ij} = N_{ij}/S_{ij} \tag{12}$$

$$P_{ij} = G_{ij} \Big/ \sum_{j=1}^{m} G_{ij} \tag{13}$$

$$H_i = -\left(\sum_{j=1}^{m} P_{ij} \ln(P_{ij})\right) \Big/ \ln(m) \tag{14}$$

$$W_i = (1 - H_i) \Big/ \left(n - \sum_{i=1}^{n} H_i\right) \qquad \text{v} \tag{15}$$

where n is the number of geothermal evidence factor, m is the class of geothermal evidence layer.

3.3 Index Overlay Model

The Index Overlay (IO) Model needs to determine the optimal threshold and weight coefficient. The evidence layer is first binarized through the optimal threshold, and then the geothermal favorability map is obtained by superimposing each binarization map. In order to avoid the influence of subjective factors, the IO model assigns the same weight coefficient to all evidence factors. The output value V, which represents the geothermal potential, is calculated by Eq. (16).

$$V = \frac{\sum_{i=1}^{n} W_i B_i}{\sum_{i=1}^{n} W_i} \tag{16}$$

where B_i is the value of each grid cell of the binary map corresponding to the evidence layer i.

4.GEOTHERMAL EVIDENCE LAYERS

4.1 Training points

There are 320 geothermal wells in Xiong'an New Area, including 159 geothermal wells exploiting carbonate reservoir of the Jixian system (Fig. 2a).

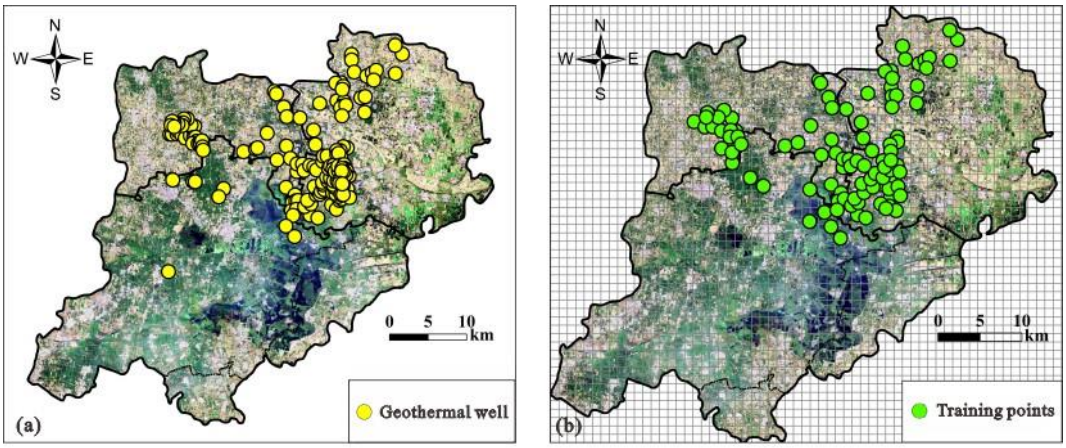

Figure 2: Distribution of the geothermal well exploiting the carbonate reservoir of the Jixian system (a) and the training points (b).

As the adjacent geothermal wells may belong to the same geothermal system, it is assumed that the geothermal wells distributed within 1 km × 1 km belong to the same geothermal system. Based on this assumption, the geothermal wells with the temperature of no less than 40 °C at the depth of 1000 m is selected as the training points. A total of 101 training points has been selected in Xiong'an New Area for the evaluation of geothermal resource potential (Fig. 2b).

4.2 Distance to the Major Grabens

The high Bouguer gravity gradient is usually related to geothermal activity. The Bouguer gravity value in Xiong'an New Area is -14 ~ 24 mGal. The uplift has high Bouguer gravity value. The Bouguer gravity value of the Niutuozhen uplift and Rongcheng uplift in the north of the new area is 0~24 mGal. The spatial distribution of the Bouguer gravity value shows that there is no obvious spatial connection between Bouguer gravity value and geothermal occurrence (Fig. 3a). The area with Bouguer gravity gradient greater than 0.238 (average value + standard deviation) is defined as the major grabens in Xiong'an New Area. Euclidean distance analysis is conducted to obtain the distance to the major graben (Fig. 3b). 78% of the training points (79 training points) are located within 5 km from the major graben. Only 2% of the training points (2 training points) are more than 10 km away from the major graben.

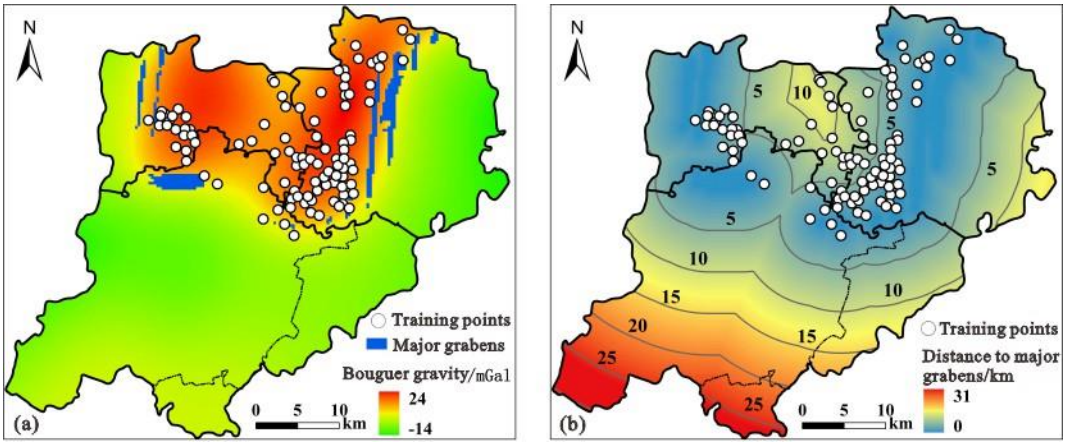

Figure 3: (a) The bouguer gravity anomaly map. (b) Distance to the major graben.

4.3 Depth of the Basement

The upward transmission of deep terrestrial heat flow in Xiong'an New Area is affected by the depth of basement. The depth of the basement in Xiong'an New Area is shown in Fig. 4a. Statistics show that 99% of the training points (100 training points) are distributed in the area where the depth of the basement is less than 3 km.

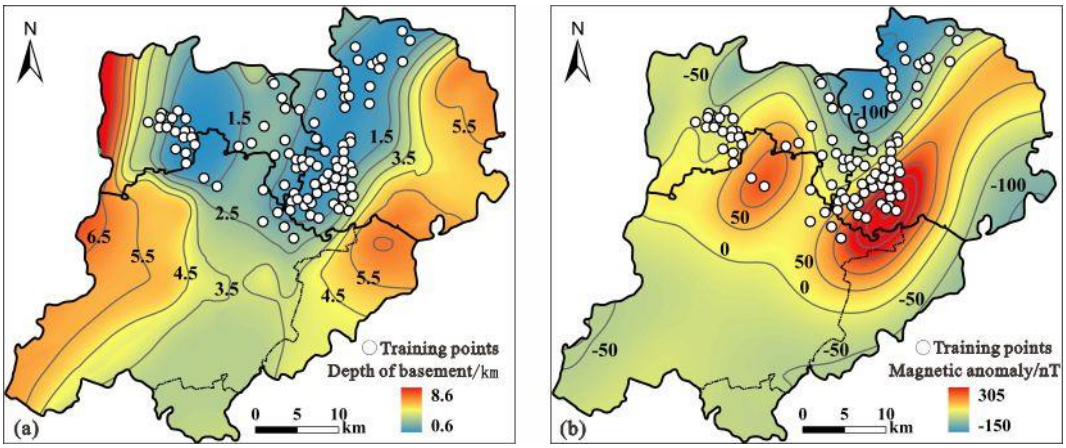

Figure 4: (a) The depth of the basement. (b) Magnetic anomaly map.

4.4 Magnetic Anomaly

As shown in Fig. 4b, most of the training points in Xiong'an New Area are distributed in areas with high magnetic anomaly. 53% of the training points (47 training points) are located in areas with magnetic anomaly value greater than -10 nT.

4.5 Geothermal Gradient

Fig. 5a shows the distribution of geothermal gradient in Xiong'an New Area. The geothermal gradient at the axis of the uplift reaches 85.9 °C·km^{-1}, and 88% of the training points (89 training points) are located in the area where the geothermal gradient is greater than 30 °C·km^{-1}.

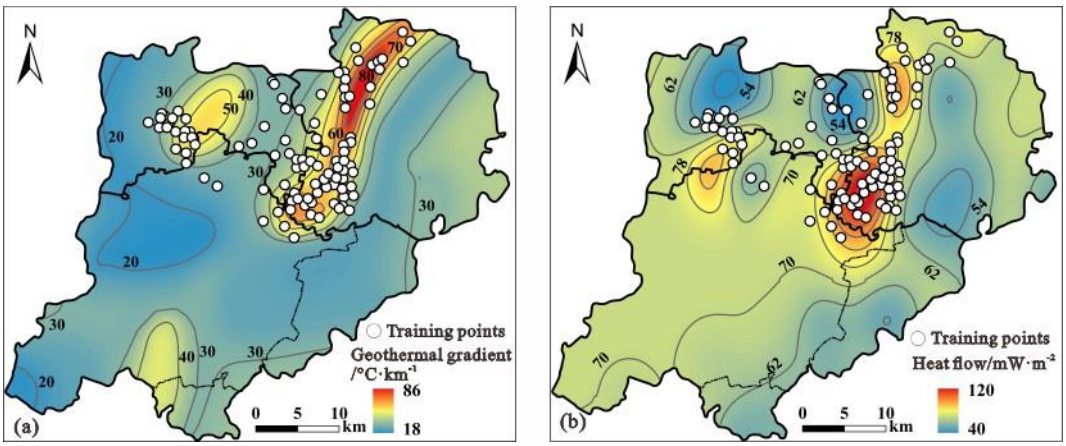

Figure 5: (a) Geothermal gradient map. (b) Terrestrial heat flow map.

4.6 Terrestrial Heat Flow

It can be seen from Fig. 5b that there is a clear spatial connection between the training points and the terrestrial heat flow in Xiong'an New Area. 71% of the training points (72 training points) are located in areas with terrestrial heat flow greater than 69.0 $mW \cdot m^{-2}$ (average terrestrial heat flow in Bohai Bay Basin), and 82% of the training points (83 training points) are located in areas with terrestrial heat flow greater than 60.4 $mW \cdot m^{-2}$ (average terrestrial heat flow in the continent of China).

5.RESULTS

5.1 Geothermal Favorability

5.1.1 Weights of Evidence Model

To ensure the calculation efficiency, all evidence layers are divided into 0.1 km × 0.1 km pixels. The average standard deviation method and weights of evidence method are used to determine the threshold of the binary prediction map. The evidence factor value corresponding to 101 training points in each evidence layer and the threshold of each evidence factor determined by the average standard deviation method are shown in Table 1.

Table 1: Evidence factor value and threshold calculated based on the average standard deviation method

Evidence factor	Min	Max	Average value	Standard deviation	Threshold
Distance to major graben/km	0.00	10.58	3.50	2.62	0.88~6.12
Depth of basement/km	0.71	3.19	0.54	1.30	0.76~1.84
Magnetic anomaly/nT	-145.18	301.71	14.10	109.04	-94.94~123.15
Geothermal gradient/$°C \cdot km^{-1}$	25.71	84.96	48.78	14.35	34.43~63.13
Heat flow/$mW \cdot m^{-2}$	46.37	119.63	80.20	17.92	62.27~98.12

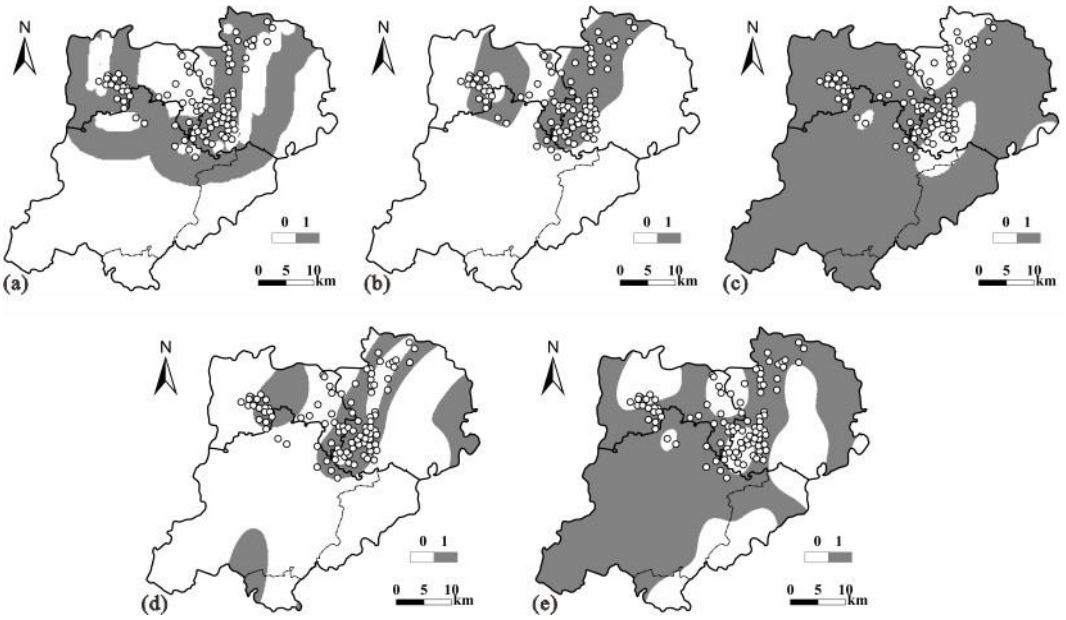

Figure 6: The binary prediction map of five evidence layers based on the average standard deviation method. (a) Distance to the major graben. (b) Depth of basement. (c) Magnetic anomaly. (d) Geothermal gradient. (e) Terrestrial heat flow.

The binary prediction map obtained based on the average standard deviation method is shown in Fig. 6. Table 2 shows the corresponding weight coefficient W^+ and W^-, contrast C and standardized contrast $S(C)$ calculated according to the weights of evidence method. Binary prediction map of the evidence layer is constructed according to the maximum value of $C/S(C)$. It can be seen that the basement depth and geothermal gradient are most closely related to the geothermal occurrence. The binary prediction map obtained based on the weights of evidence method is shown in Fig. 7.

Table 2: The weight coefficient and threshold of different evidence factors based on the weights of evidence method

		Class										
Distance to the major graben		<0.9	<2.0	<3.0	**<4.0**	<4.9	<5.8	<6.7	<7.6	<8.5	<9.5	<10.0
	W^+	0.465	0.596	0.600	**0.748**	0.636	0.549	0.501	0.457	0.394	0.345	0.348
	$S^2(W^+)$	0.063	0.029	0.020	**0.014**	0.013	0.012	0.012	0.011	0.011	0.011	0.010
	W^-	-0.068	-0.205	-0.366	**-0.894**	-0.989	-1.038	-1.238	-1.467	-1.565	-1.727	-2.744
	$S^2(W^-)$	0.012	0.015	0.020	**0.037**	0.045	0.053	0.071	0.100	0.125	0.167	0.500
	C	0.532	0.802	0.966	**1.642**	1.625	1.588	1.738	1.923	1.959	2.072	3.092
	$C/S(C)$	1.953	3.806	4.853	**7.301**	6.740	6.234	6.036	5.773	5.317	4.922	4.330
Depth of basement		<0.9	<1.1	**<1.3**	<1.5	<1.7	<1.9	<2.1	<2.3	<2.6	<2.9	<3.0
	W^+	1.284	1.526	**1.477**	1.376	1.326	1.281	1.222	1.179	1.116	1.061	0.961
	$S^2(W^+)$	0.050	0.020	**0.015**	0.014	0.013	0.012	0.011	0.010	0.010	0.010	0.010
	W^-	-0.164	-0.587	**-0.898**	-1.018	-1.211	-1.519	-2.105	-2.879	-3.134	-3.508	-4.139
	$S^2(W^-)$	0.012	0.020	**0.029**	0.033	0.042	0.059	0.111	0.250	0.333	0.500	1.000
	C	1.448	2.113	**2.376**	2.394	2.537	2.801	3.327	4.058	4.250	4.569	5.100
	$C/S(C)$	5.794	10.610	**11.356**	10.991	10.848	10.529	9.524	7.953	7.251	6.397	5.075
Magnetic anomaly		>-140	>-125.8	>-102.7	>-78.9	>-55.8	>-37.9	>-23.8	>-6.6	>13.5	>35.8	**>50**
	W^+	-0.021	-0.056	-0.081	-0.163	-0.144	-0.010	0.121	0.209	0.252	0.410	**0.466**
	$S^2(W^+)$	0.010	0.011	0.011	0.013	0.013	0.014	0.016	0.019	0.024	0.029	**0.035**
	W^-	0.726	0.890	0.847	0.918	0.639	0.023	-0.160	-0.189	-0.147	-0.157	**-0.140**
	$S^2(W^-)$	0.250	0.111	0.077	0.044	0.040	0.032	0.025	0.021	0.017	0.015	**0.014**
	C	-0.747	-0.946	-0.928	-1.081	-0.784	-0.033	0.281	0.399	0.400	0.567	**0.606**
	$C/S(C)$	-1.463	-2.708	-3.121	-4.554	-3.398	-0.151	1.379	1.999	1.980	2.693	**2.755**
Geothermal gradient		>31.0	>33.1	>35.0	>36.4	>38.1	>39.6	**>41.0**	>42.5	>46.1	>49.6	>53.1
	W^+	0.415	0.473	0.606	0.790	0.909	1.024	**1.443**	0.910	1.005	1.120	1.136
	$S^2(W^+)$	0.010	0.010	0.010	0.011	0.012	0.012	**0.015**	0.014	0.017	0.018	0.023
	W^-	-3.555	-2.979	-2.763	-1.787	-1.323	-1.280	**-0.918**	-0.290	-0.240	-0.228	-0.171
	$S^2(W^-)$	1.000	0.500	0.333	0.100	0.056	0.050	**0.029**	0.008	0.007	0.007	0.006
	C	3.970	3.452	3.369	2.578	2.231	2.304	**2.362**	1.199	1.245	1.348	1.306
	$C/S(C)$	3.950	4.833	5.747	7.736	8.581	9.226	**11.210**	8.132	8.058	8.498	7.578
Heat flow		>58.0	>59.8	>63.2	>66.3	>68.9	>71.4	**>73.9**	>77.0	>80.5	>84.1	>87.9
	W^+	0.008	0.031	0.017	0.092	0.208	0.774	**0.954**	1.028	1.106	1.265	1.366
	$S^2(W^+)$	0.006	0.006	0.007	0.007	0.008	0.011	**0.012**	0.015	0.019	0.022	0.029
	W^-	-0.044	-0.128	-0.041	-0.165	-0.257	-0.397	**-0.356**	-0.269	-0.216	-0.189	-0.147
	$S^2(W^-)$	0.035	0.028	0.018	0.015	0.013	0.010	**0.008**	0.007	0.007	0.006	0.006
	C	0.052	0.159	0.058	0.257	0.465	1.172	**1.310**	1.297	1.322	1.454	1.513
	$C/S(C)$	0.257	0.863	0.367	1.711	3.205	8.268	**9.104**	8.583	8.238	8.573	8.115

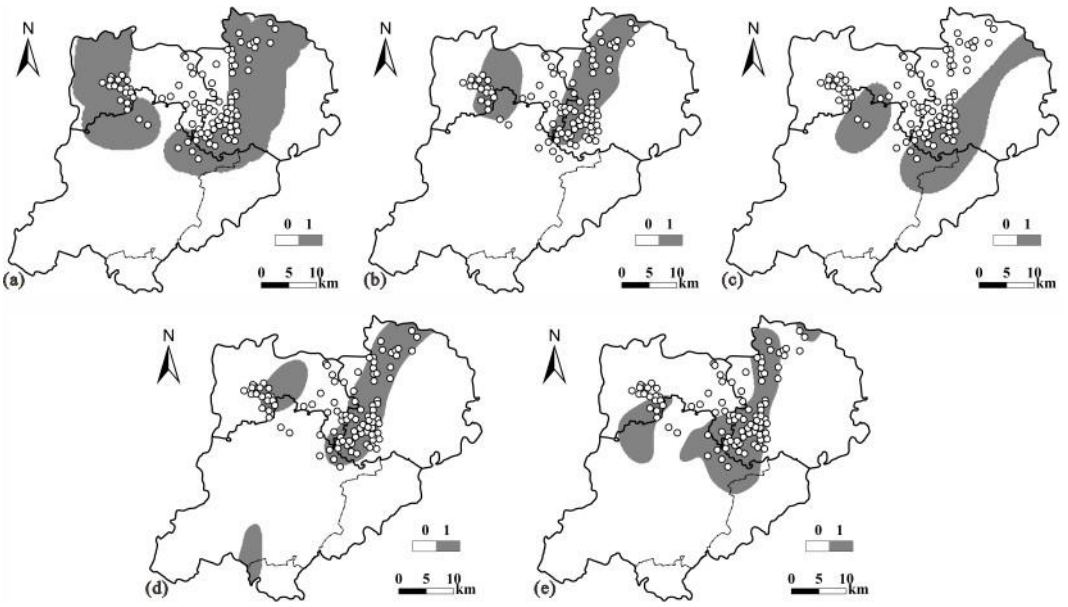

Figure 7: The binary prediction map of five evidence layers based on the weights of evidence method. (a) Distance to the major graben. (b) Depth of basement. (c) Magnetic anomaly. (d) Geothermal gradient. (e) Terrestrial heat flow.

The independence of evidence factors is analyzed by χ^2 test. The χ^2 value between pairs of evidence factors is shown in Table 3. The degree of freedom is determined as (2-1) × (2-1)=1, the significance level α is 0.02, the critical χ^2 value $\chi_{1,0.98}^2$ is 5.412. The results show that 90% of χ^2 value is less than the critical χ^2 value, indicating that there is no obvious conditional dependence between the evidence factors.

Table 3: Chi square value of conditional independence test of evidence factors

	Average standard deviation method				Weights of evidence method			
	Distance to the major graben	Depth of basement	Magnetic anomaly	Geothermal gradient	Distance to the major graben	Depth of basement	Magnetic anomaly	Geothermal gradient
Heat flow	0.009	1.012	0.615	1.663	1.914	3.690	1.008	8.093
Distance to the major graben	—	0.087	0.001	0.025	—	2.967	2.066	1.333
Depth of basement	—	—	1.989	1.378	—	—	0.502	1.664
Magnetic anomaly	—	—	—	0.292	—	—	—	0.009

The prior probability P(G)=101/177290=0.00057. The posterior probability calculated by the average standard deviation method with the WofE model is 0.0000346~0.0274. The area with a posterior probability less than 0.00057 is classified as low favorable area, and the area with a posterior probability greater than 0.00057 is classified as medium favorable area, high favorable area and extremely high favorable area according to the natural breaks (Jenks) method. The geothermal favorability map obtained by the average standard deviation method with the WofE model is shown in Fig. 8a. The posterior probability calculated by the weights of evidence method with the WofE model is 0.0000135~0.117. The area with a posterior probability less than 0.00057 is classified as low favorable area, and the area with a posterior probability greater than 0.00057 is classified as medium favorable area, high favorable area and extremely high favorable area according to the natural breaks (Jenks) method. The geothermal favorability map obtained by the weights of evidence method with the WofE model is shown in Fig. 8b.

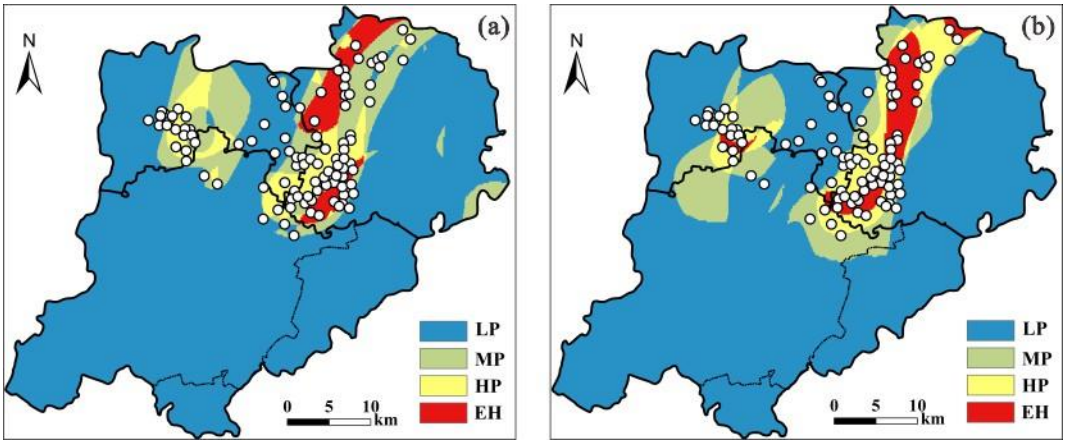

Figure 8: The geothermal favorability map obtained by the average standard deviation method (a) and the weights of evidence method with the WofE model. LP is low favorable area, MP is medium favorable area, HP is high favorable area, EH is extremely high favorable area.

5.1.2 Weighted Information Content Model

The classification of each evidence factor during the evaluation of geothermal potential by the WIC model shown in Table 4 is based on Table 2. The information content I_i is calculated according to Eq. (10). The information entropy and weight coefficient of five evidence factors, namely distance to major graben, depth of basement, magnetic anomaly, geothermal gradient and terrestrial heat flow, are calculated based on the information entropy theory.

The total weighted information content is -0.809 ~ 0.379 (Fig.9a). The weighted information content value of each training point is counted, and then the relation curve of information content value and cumulative percentage of number of training points is plotted as shown in Fig.10. The corresponding information content value at the inflection point of the curve (-0.0737, 0.0563 and 0.263) is set as the threshold of the geothermal favorability map shown in Fig 9b.

Table 4: Classification of the evidence factors and its connection with training points

		Class											
		1	2	3	4	5	6	7	8	9	10	11	12
Distance to the major graben	Area/km^2	176.5	152.3	153.0	133.0	119.7	96.6	94.7	86.2	89.1	79.7	46.1	545.5
	N_{ij}	16	18	16	24	5	3	5	4	2	2	4	2
	I_i	0.67	1.05	0.88	1.66	-0.45	-0.88	-0.11	-0.30	-1.34	-1.18	0.61	-3.96
Depth of basement	Area/km^2	97.4	97.6	69.9	50.5	44.1	50.5	66.7	47.6	39.9	37.7	70.2	1100.8
	N_{ij}	20	31	15	7	4	7	8	5	1	1	1	1
	I_i	1.85	2.48	1.91	1.28	0.67	1.28	1.07	0.88	-1.18	-1.10	-2.00	-5.97
Magnetic anomaly	Area/km^2	34.0	30.9	33.0	63.4	70.3	300.1	291.8	194.1	181.9	176.5	76.9	319.3
	N_{ij}	4	5	4	10	2	6	9	8	11	8	5	29
	I_i	1.05	1.51	1.09	1.47	-1.00	-1.51	-0.89	-0.47	0.09	-0.33	0.19	0.67
Geothermal gradient	Area/km^2	616.3	76.7	144.8	214.8	138.2	77.0	60.1	58.9	72.0	28.7	14.1	279.5
	N_{ij}	1	1	1	7	8	2	4	3	1	5	1	67
	I_i	-5.13	-2.12	-3.04	-0.80	0.03	-1.13	0.23	-0.15	-2.03	1.62	0.33	2.08
Heat flow	Area/km^2	268.7	50.8	83.8	75.8	74.9	84.6	107.5	116.6	134.2	404.1	57.3	315.0
	N_{ij}	13	1	5	0	3	1	0	2	6	2	1	67
	I_i	-0.24	-1.53	0.07	0	-0.51	-2.27	0	-1.73	-0.35	-3.52	-1.71	1.90

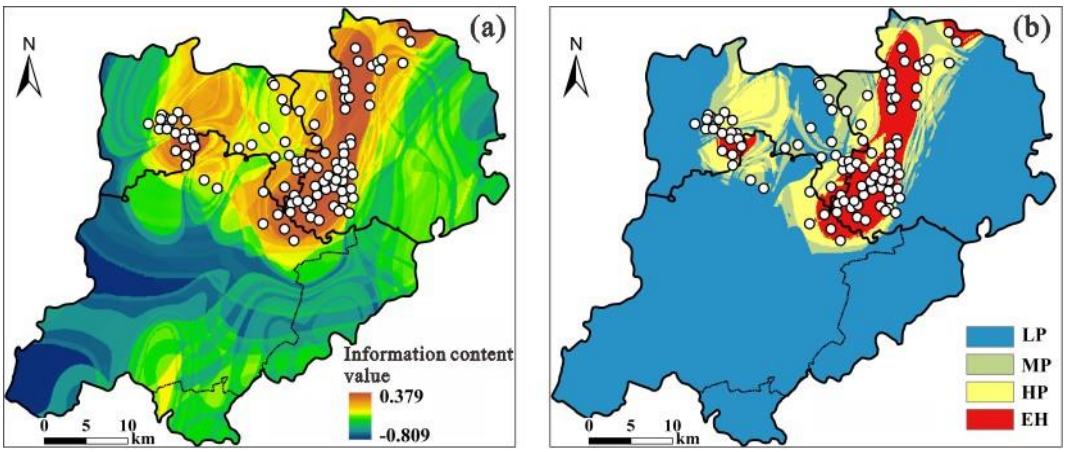

Figure 9: (a) Distribution of information content value. (b)The geothermal favorability map obtained by the WIC model. LP is low favorable area, MP is medium favorable area, HP is high favorable area, EH is extremely high favorable area.

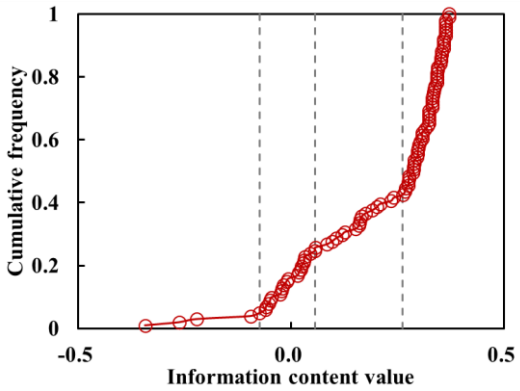

Figure 10: The relationship between the cumulative frequency of the number of training points and the information content value.

5.1.2 Index Overlay Model

The IO model assumes that the five evidence factors have the same impact on geothermal occurrence. Each evidence layer obtained in Section 5.1.1 is given a weight coefficient of 0.2, and the geothermal favorability map is reclassified into four class.

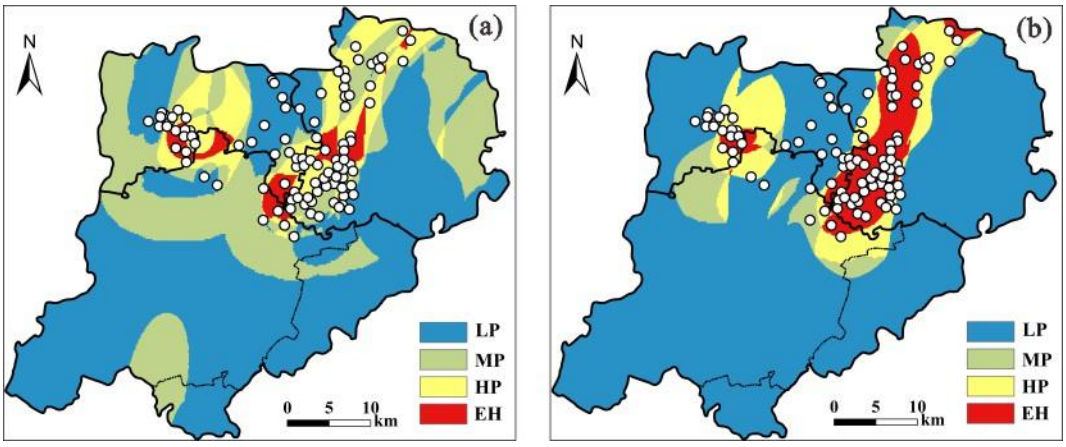

Figure 11: The geothermal favorability map obtained by the average standard deviation method (a) and the weights of evidence method with the IO model. LP is low favorable area, MP is medium favorable area, HP is high favorable area, EH is extremely high favorable area.

The potential value of geothermal favorability map obtained by the average standard deviation method is 0.2~1.0. The potential value less than 0.4 is defined as low favorable area, the potential value between 0.4~0.6 is defined as medium favorable area, the potential value between 0.6~0.8 is defined as high favorable area, and the potential value greater than 0.8 is defined as extremely high favorable area. The potential value of geothermal favorability map obtained by the weights of evidence method is 0~0.00183. The potential value less than the prior probability 0.00057 is determined as low favorable area, and the potential value greater than 0.00057 is

divided into medium favorable area, high favorable area and extremely high favorable area according to the natural breaks method. The geothermal favorability map based on the IO model is shown in Fig.11.

5.1.4 Model Test

1) Kappa coefficient analysis

Some kappa coefficients of the evaluation results are shown in Table 5. The kappa coefficient between the evaluation results of the WofE model and IO model with the weights of evidence binary map is the greatest (0.71). It indicates that the evaluation results of these two methods are almost consistent, and there is highly consistency for low favorable areas and medium favorable areas. According to the statistics of the coincidence of the evaluation results of each grid cell, the coincidence corresponding to the two models with the highest kappa coefficient is more than 80%.

Table 5: Kappa analysis of the consistency of the favorability maps

		WofE-WofE							IO- WofE				
		LP	MP	HP	EH	Sum			LP	MP	HP	EH	Sum
IO-WofE	LP	135077	0	0	0	135077	WIC	LP	123238	5255	2748	0	131241
	MP	2101	6847	0	0	8948		MP	9058	1147	4473	93	14771
	HP	0	12004	5428	0	17432		HP	2781	2487	9247	792	15307
	EH	0	0	5892	8764	14656		EH	0	59	964	13771	14794
	Sum	137178	18851	11320	8764	176113		Sum	135077	8948	17432	14656	176113
	K	*K(LP)*	*K(MP)*	*K(HP)*	*K(EP)*			*K*	*K(LP)*	*K(MP)*	*K(HP)*	*K(EP)*	
	0.71	1.00	0.74	0.26	0.58			0.60	0.74	0.03	0.56	0.92	
		WofE-WofE							WofE-ASD				
		LP	MP	HP	EH	Sum			LP	MP	HP	EH	Sum
WIC	LP	124655	6521	65	0	131241	WIC	LP	127760	2977	274	230	131241
	MP	9564	3805	1402	0	14771		MP	6880	5571	1329	991	14771
	HP	2959	8313	4035	0	15307		HP	3452	7016	3236	1603	15307
	EH	0	212	5818	8764	14794		EH	318	5829	5073	3574	14794
	Sum	137178	18851	11320	8764	176113		Sum	138410	21393	9912	6398	176113
	K	*K(LP)*	*K(MP)*	*K(HP)*	*K(EP)*			*K*	*K(LP)*	*K(MP)*	*K(HP)*	*K(EP)*	
	0.51	0.77	0.17	0.21	0.57			0.48	0.88	0.29	0.16	0.21	

2) Success index analysis

Table 6 shows the success indexes of evaluation results for different models. It can be seen that the success indexes of high favorable area (HP) and extremely high favorable area (EH) are greater than the priori probability. The success indexes of the WIC model, the WofE model and IO model are the largest for the extremely high favorable area, indicating that the model can better evaluate the high favorable area and extremely high favorable area. The success index is high in extremely high favorable area and high favorable area, and the success index is low in low favorable area. It indicates that the evaluation results of all models are consistent with the actual distribution of geothermal resource. The success index is the highest for the extremely high favorable area evaluated by the weights of evidence binary map predicted by the WofE model and the WIC model, which are 0.468% and 0.392%, respectively.

Table 6: Success index for the favorability maps

Model	Binary method	*SI*/%			
		LP	MP	HP	EH
WofE	ASD	0.014	0.173	0.303	0.219
	WofE	0.017	0.069	0.212	0.468
WIC		0.004	0.129	0.124	0.392
IO	ASD	0.023	0.035	0.241	0.248
	WofE	0.017	0.022	0.109	0.389

3) Receiver operating characteristic curve analysis

The receiver operating characteristic (ROC) curve corresponding to the evaluation results of geothermal potential based on different models is shown in Fig.12. The area under curve (AUC) corresponding to the binarization of the average standard deviation method with the WofE model, the binarization of the weights of evidence method with the WofE model, the WIC model, the binarization of the average standard deviation method with the IO model, and the binarization of the weights of evidence method with the IO model are 0.791, 0.805, 0.854, 0.728, and 0.797, respectively. It can be seen that the AUC values of all models are greater than 0.7, indicating a high accuracy of the evaluation results. The WIC model has the highest accuracy, followed by the WofE model and the IO model.

According to the evaluation results of geothermal potential based on the WIC model, the extremely high favorable area and high favorable area in Xiong'an New Area contain 76.2% of the training points (77), covering an area of 148.1 km^2 and 152.8 km^2, respectively, and accounting for 8.4% and 8.7% of the total area of Xiong'an New Area. The extremely high favorable area and high favorable area are mainly distributed in Niutuo Town uplift and Rongcheng uplift in the south of Rongcheng County.

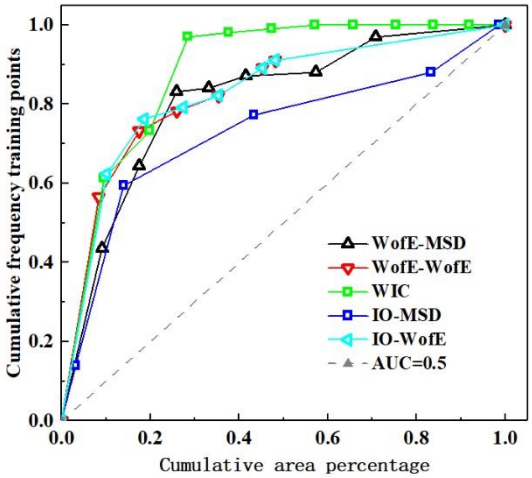

Figure 12: The receiver operating characteristic (ROC) curves of all models.

5.2 Amount of Thermal Energy

5.2.1 Parameter identification

1) Evaluation area

The evaluation area derived from the distribution of carbonate reservoirs in the Jixian System of Wumishan Formation in Xiong'an New Area is 1059.2 km^2 (Fig. 13a). Divide the evaluation area into 0.1 km × 0.1 km grid cells, and then calculate the amount of thermal energy in the carbonate reservoirs.

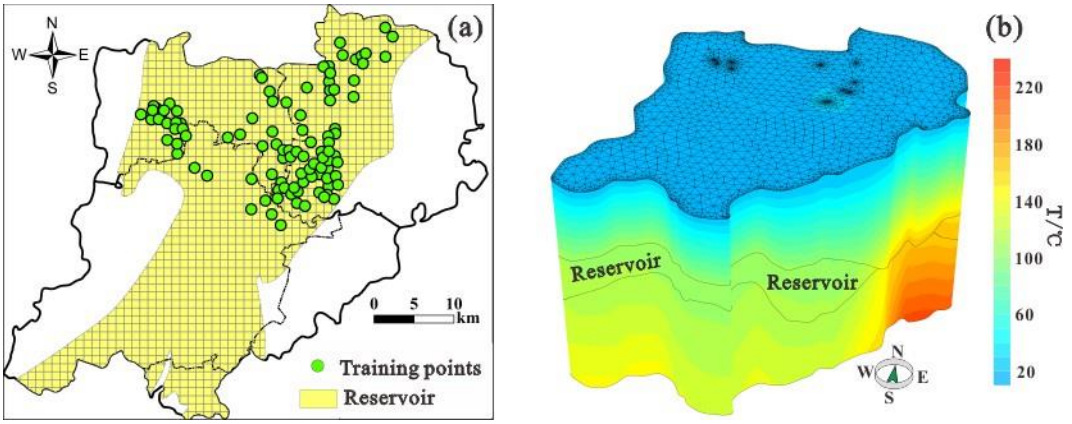

Figure 13: (a) Division of evaluation area. (b) Temperature distribution of reservoir.

2) Thickness of carbonate reservoir

The steady temperature measured in the carbonate reservoir of Xiong'an New Area presents convective characteristics, indicating that the carbonate reservoir is rich in geothermal fluid. The effective thermal reservoir is usually distributed in the upper Jixian System. The reservoir thickness accounts for 20%~40% of the thickness of the Jixian System.

3) Reservoir temperature and strata parameter

The temperature of the reservoir is obtained from the simulation results of the steady-state temperature field of the lithosphere. The temperature distribution within the depth of 10 km in Xiong'an New Area is shown in Fig. 13b. The hydrogeological and thermophysical parameters of each stratum are shown in Table 7.

Table 7: The hydrogeological and thermophysical parameters of each stratum

Stratum	Hydraulic conductivity /m·d^{-1}			porosity	Volume heat capacity of rock /MJ·m^{-3}·K^{-1}	Thermal conductivity of rock /W·m^{-1}·K^{-1}
	K_x	K_y	K_z			
Q	0.05	0.05	0.005	0.2	1.82	1.5
N*m*	0.25	0.25	0.025	0.15	2.39	1.7
E	0.25	0.25	0.025	0.15	2.39	1.7
Jx*w*	1.14	1.14	0.0114	0.05	2.52	4.6
Pz	0.01	0.01	0.001	0.02	1.93	3

5.2.2 Results

The amount of thermal energy of carbonate reservoir in Xiong'an New Area is shown in Table 8. The amount of thermal energy of the carbonate reservoir of Jixian System is 32.9~65.8 EJ, equivalent to 1.1~2.2 × 10^9 t standard coal, which may reduce CO_2 emissions by 2.5~5.1 × 10^9 t. The recovery rate is 0.15, the recoverable amount of thermal energy is 0.02~369.6 TJ/grid unit, and the total recoverable amount of thermal energy is 4.9~9.9 EJ, equivalent to 0.2~0.3 × 10^9 t standard coal, which may reduce CO_2 emissions by 0.4~0.8 × 10^9 t. Fig. 14 shows the distribution of the recoverable amount of thermal energy in the carbonate reservoir of Jixian System in Xiong'an New Area.

Table 8: The amount of thermal energy of carbonate reservoir in Xiong'an New Area

Reservoir	Total thermal energy /EJ	Recoverable thermal energy/EJ	Recoverable thermal energy equivalent to standard coal/10^9 t	Recoverable thermal energy equivalent to CO_2 emissions/10^9 t
Jx*w*	32.9~65.8	4.9~9.9	0.2~0.3	0.4~0.8

The recoverable amount of thermal energy in the extremely high favorable area assessed by the WIC model is 16.8~185.3 TJ/grid unit, with a total amount of 0.6~1.2 EJ. The recoverable amount of thermal energy in the high favorable area assessed by the WIC model is 11.8~250 TJ/grid unit, with a total amount of 0.7~1.3 EJ.

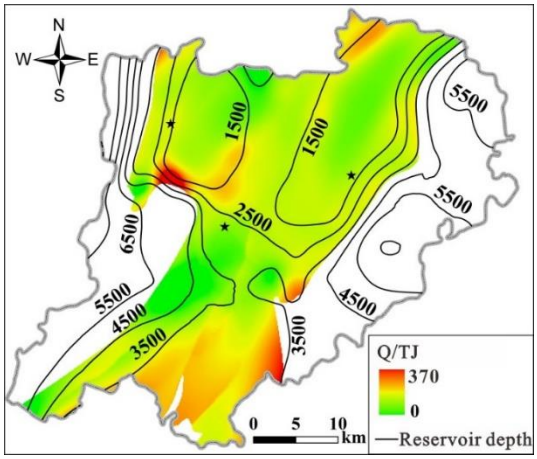

Figure 14: Distribution of the recoverable amount of thermal energy in Xiong'an New Area

6.CONCLUSION

In this paper, two data-driven models (the WofE model and the WIC model) and one knowledge-driven model (IO model) are used to evaluate the geothermal potential of Xiong'an New Area based on ArcGIS platform. The amount of thermal energy is also calculated using the unit volumetric method. The main conclusions are as follows:

1) In Xiong'an New Area, 78% of the training points are distributed within the distance less than 5 km from the major graben, 99% of the training points are distributed within the area with basement depth less than 3 km, 53% of the training points are distributed within the area with magnetic anomaly greater than -10 nT, 88% of the training points are distributed within the area with geothermal gradient greater than 30 ºC·km^{-1}, and 71% of the training points are distributed within the area with terrestrial heat flow greater than 69.0 mW·m^{-2}. The basement depth and geothermal gradient are most closely related to the geothermal occurrence in Xiong'an New Area.

2) The evaluation results of weights of evidence binary method with the WofE model and the WIC model are consistent with the actual geothermal occurrence in Xiong'an New Area, and the WIC model is the most effective and accurate. The extremely high favorable area and high favorable area contain 76.2% of the training points, covering an area of 148.1 km^2 and 152.8 km^2, respectively, and accounting for 8.4% and 8.7% of the total area. The extremely high favorable area and high favorable area mainly distributed in Niutuo Town uplift and Rongcheng uplift in the south of Rongcheng County.

3) The total amount of thermal energy in the carbonate reservoir of Jixian System is 32.9~65.8 EJ, of which recoverable amount is 4.9~9.9 EJ. The recoverable amount is equivalent to 0.2~0.3 × 10^9 t standard coal and may reduce CO_2 emissions by 0.4~0.8 × 10^9 t. Moreover, the recoverable amount of thermal energy in the extremely high favorable area is 0.6~1.2 EJ, and the recoverable amount of thermal energy in the high favorable area is 0.7~1.3 EJ.

ACKONWLEDGEMENT

This work was funded by the Enterprise Commissioned Project of Sinopec Green Energy Geothermal Development Co. Ltd. (grant number 2017-016) and Key Research and Development Project of Shaanxi Province (grant number 2022ZDLSF07-06). The authors would like to express sincere gratitude to the editors and anonymous reviewers for offering constructive comments and suggestions.

REFERENCES

British Petroleum. bp statistical review of world energy. UK: British Petroleum (2022).

Muffler P. and Cataldi R.: Methods for regional assessment of geothermal resources, *Geothermics*, **7**(2-4), (1977), 53-89.

Rybach L. and Muffler L.: Geothermal systems: Principles and case histories. New York, Chichester (1980).

Prol-Ledesma R. M.: Evaluation of the reconnaissance results in geothermal exploration using GIS, *Geothermics*, **29**(1), (2000), 83-103.

Carter B.: Geographic Information Systems for Geoscientists: Modelling with GIS, *Computers & Geosciences*, (1994).

Coolbaugh M. F. and Shevenell L. A.: A method for estimating undiscovered geothermal resources in Nevada and the Great Basin, *Transactions - Geothermal Resources Council*, **28**, (2004), 13-18.

Coolbaugh M. F., Raines G. L. and Zehner R. E.: Assessment of Exploration Bias in Data-Driven Predictive Models and the Estimation of Undiscovered Resources, *Natural Resources Research*, **16**(2), (2007), 199-207.

Tuefekci N., Suezen M. L. and Guelec N.: GIS based geothermal potential assessment: A case study from Western Anatolia, Turkey, *Energy*, **35**(1), (2010), 246-261.

Sadeghi B. and Khalajmasoumi M. J. R.: A futuristic review for evaluation of geothermal potentials using fuzzy logic and binary index overlay in GIS environment, *Renewable Sustainable Energy Reviews*, **43**, (2015), 818-831.

Francesco T., Sara K., Mohamed E., et al.: Suitability Evaluation of Specific Shallow Geothermal Technologies Using a GIS-Based Multi Criteria Decision Analysis Implementing the Analytic Hierarchic Process, *Energies*, **11**(457), (2018), 1-21.

Zhang Y., Zhang Y. J., Yu H., et al.: Geothermal resource potential assessment of Fujian Province, China, based on geographic information system (GIS) -supported models, *Renewable Energy*, **153**, (2020), 564-579.

Wang Z., Zhang C., Jiang G., et al.: Effect of different exploitation schemes on production performance from the carbonate reservoir: A case study in Xiong'an new area *Journal of cleaner production*, **314**, (2021).

Gaofan Y., Guiling W., Feng M., et al.: The thermal state and geothermal energy accumulation mechanism in the Xiong'an New Area, China, *Energy Exploration Exploitation*, **37**(3), (2019), 014459871984074.

Wang Z.: Thermal regime of the lithosphere and geothermal potential in Xiong'an New Area, (2018).

Guo S., Zhu C., Qiu N., et al.: Present Geothermal Characteristics and Influencing Factors in the Xiong'an New Area, North China, *Energies*, **12**(3884), (2019), 1-22.

Agterberg F. P., Bonham-Carter G. F. and Wright D. F.: Statistical pattern integration for mineral exploration, *Computer Applications in Resource Estimation*, (1990), 1-19.

Shannon C. E.: A Mathematical Theory of Communication, *Bell System Technical Journal*, **27**(3), (1948), 379-423.